EURASIP Journal on
Wireless Communications and Networking
a SpringerOpen Journal

RESEARCH Open Access

Coordinated TDD-Underlay for Self-organizing Femtocells in Two-Tier Coexistence Scenarios

Carlos HM de Lima*, Mehdi Bennis and Matti Latva-aho

Abstract

In this contribution, we investigate the concept of time division duplexing (TDD) mode as an alternative to underlay short-range femtocells on the uplink of legacy macrocell deployments. To mitigate the resulting co-channel interference, the underlaid femtocell tier uses a distributed mechanism which is based on regular busy tones and relies on minimal signaling exchange. Stochastic geometry is used to model practical scenarios by capturing network dynamics and channel variations. The impact of the fading correlation on the performance of the coordination mechanism is examined as well. Higher-order statistics through the cumulants concept are used to recover the distribution of the co-channel interference and evaluate the system performance in terms of the outage probability and average channel capacity. We observe that our analytical framework matches well with numerical results obtained using Monte Carlo simulations. In contrast to the uncoordinated frequency division duplexing mode, the coordinated TDD-underlay solution shows a reduction in the outage probability of nearly 80%, while the average spectral efficiency increases by approximately 90% in high loads.

1 Introduction

Lately, the femtocell concept has emerged as a promising solution to achieve the stringent requirements of the next generation of cellular systems owing to the intrinsic better link quality of short range communications. Femtocells indeed constitute an inexpensive alternative to provide better indoor coverage, fairness at cell border and offloading of the overlaid macrocells [1,2]. Unfortunately, the unplanned deployment and uncoordinated operation of such small cells leads to harsh Co-channel interference (CCI) in both macro and femtocell tiers [3].

To deal with the interference problem in two-tier networks, various solutions have been proposed. For instance, López–Pérez et al. first characterize the cross-tier interference problem and then provide a comprehensive summary of candidate solutions wherein the use of dynamic spectrum allocation in conjunction with self-configuration and optimization of femtocells play a determinant role [4]. Similarly, a sub-band scheduling and interference cancelation mechanism is proposed in [5] by which the macrocell bandwidth is partitioned and femtocells use load-spillage to control their power across the sub-bands. As an alternative to the typical spectrum partitioning solutions, the time division duplexing (TDD)-underlay concept is proposed in [6] to take advantage of the natural traffic asymmetry between the downlink (DL) and uplink (UL), as well as the user spatial diversity. Unfortunately, time-multiplexed communicating links operating in universal frequency reuse are still exposed to the CCI generated by dominant interferers transmitting in an uncoordinated manner. Thus, we augment the TDD-underlay concept by incorporating a distributed mechanism which dynamically coordinates inter-cell time-slot allocation to avoid strong interference from nearby conflicting transmitters [5,7].

In this study, the coordination policy consists of a decision criterion (whether to coordinate or not) and an interference avoidance algorithm. According to the adopted policy, short-range femtocells then coordinate their transmissions with co-channel interferers by means of regular busy tones. Additionally, we evaluate the two-tier coexistence scenarios considering a practical radio channel propagation model which includes path loss attenuation, shadowing and multi-path fading. Furthermore, an analytical framework which captures the impact of channel variations and network dynamics on the system performance is introduced. The main contributions of this study are summarized in the following list:

*Correspondence: carlosl@ee.oulu.fi
Centre for Wireless Communications (CWC), University of Oulu, Oulu, Finland

1. Comprehensive channel model: we employ a detailed radio channel propagation model that includes path loss attenuation, log-normal (LN) shadowing and Nakagami-*m* fading as described in Section 2.
2. Analytical framework: in Section 2.4, stochastic geometry and higher-order statistics are combined into an stochastic framework which captures channel effects and network algorithms on the performance of the two-tier network under study.
3. Dynamic evaluation scenarios: by combining the channel model of Section 2 with network algorithms and strategies through the proposed framework, we examine practical evaluation scenarios as described in Section 4.
4. Coordinated TDD-underlay strategy: as described in Section 3, self-organizing femtocells communicate in the TDD mode and coordinate so as to reduce the interference that is generated towards the overlaid tier and among themselves.

In Section 5, the outage probability and average channel capacity of the tagged receiver are used to assess the performance of the two-tier coexistence scenarios under consideration. Thereafter, we draw conclusions and make final remarks in Section 6.

2 System model and analytical framework

In this section we make definitions, present assumptions and characterize our system model. Thereafter, we resort to the theory of stochastic geometry and recall the concept of spatial point processes to establish our analytical framework.

2.1 Definitions and notation

Definition 1. ***(Tagged receiver)*** *A femto base station (FBS) that is taken as the reference (typical node) to compute the CCI on the UL of the evaluation scenarios.*

Definition 2. ***(Observation region)*** *An annular region around the tagged receiver over which we account for the interference contribution. The observation region is denoted by $\mathcal{O}$ and defined by the minimum and maximum radii which are denoted by R_m and R_M, respectively.*

Definition 3. ***(Partial moment of a random variable)*** *Let Y be a random variable (RV), then $\mathrm{E}_Y\left[y_m, y_M, n\right] = \int_{y_m}^{y_M} y^n f_Y\left(y\right) \mathrm{d}y$ denotes the n^{th} partial moment of that RV with y_m and y_M denoting the lower and upper integration limits, respectively.*

2.2 Propagation channel model

Radio links are degraded by path loss and shadowed fading, which is assumed to be independent over distinct network entities and positions. A signal strength decay function, $l\left(r\right) = r^{-\alpha}$, where α is the path loss exponent, describes the path loss attenuation (unbounded path loss model [8]), while the received squared-envelop due to multi-path channel fading and shadowing is represented by a RV $X \in \mathbb{R}^+$ with cumulative distribution function and probability density function (PDF) denoted by $F_X\left(x\right)$ and $f_X\left(x\right)$, respectively. An interferer disrupts the communication of the tagged receiver with an interfering component given by

$$p_r = p\ l\left(r\right) x, \tag{1}$$

where p represents the interferer's transmit power, r is the separation distance from that interferer to the tagged receiver, and x corresponds to the channel shadowed fading.

The composite distribution of the received squared-envelop due to LN shadowing and Nakagami-*m* fading has a Gamma-LN distribution with PDF,

$$f_X(x) = \int_0^\infty \left(\frac{m}{\omega}\right)^m \frac{x^{m-1}}{\Gamma(m)} \exp\left(-\frac{m}{\omega}x\right) \times \frac{\xi}{\sqrt{2\pi}\sigma\omega} \exp\left[-\frac{\left(\xi \ln\omega - \mu_{\Omega_p}\right)^2}{2\sigma_{\Omega_p}^2}\right] \mathrm{d}\omega, \tag{2}$$

where m is the shape parameter of the Gamma distribution, $\xi = \ln\left(10\right)/10$, Ω_p is the mean squared-envelop, μ_{Ω_p} and σ_{Ω_p} is the mean and standard deviation of Ω_p, respectively.

Ho and Stüber show in [9] that a composite Gamma–LN distribution can be approximated by a single LN distribution with mean and variance (in logarithmic scale) given by

$$\mu_{\mathrm{dB}} = \xi\left[\psi\left(m\right) - \ln\left(m\right)\right] + \mu_{\Omega_p}, \tag{3}$$

$$\sigma_{\mathrm{dB}}^2 = \xi^2 \zeta\left(2, m\right) + \sigma_{\Omega_p}^2. \tag{4}$$

where $\psi\left(m\right)$ is the Euler psi function and $\zeta\left(2, m\right)$ is the generalized Riemann zeta function [10]. In what follows, we use this single LN approximation to simplify our mathematical treatment and then characterize the radio channel attenuations in various coexistence scenarios.

2.3 Network deployment model

Spatial point processes are the common approach to model and analyze random point patterns. For instance, point processes are used in statistical ecology to model locations of trees and bird nests, in astrostatistics to study the relative disposition of stars and galaxies, in stereology to provide spatial interpretations of planar sections of materials and tissues, and in wireless systems to account for the effect of the random distribution of communicating nodes in the network performance [11-15]. Herein, we use the stochastic geometry framework to model the two-tier coexistence scenarios wherein a reference macro

base station (MBS) is underlaid with FBS which operate in closed access mode [16]. The underlaid tier is composed of femtocells uniformly scattered over the network area (unplanned deployment). In other words, the homogeneous Poisson point process (PPP) Φ with density λ (FBS/m^2) in $\mathbb{R}^2$ consists of the locations of all femto base stations in the network at any given time instant. Thus, the number of active femtocells in an arbitrary region $\mathcal{R}$ of area A is a Poisson RV with parameter λA [17]. The fading effect is incorporated into the model as a random mark associated with each point of Φ [18]. By virtue of the Marking theorem [17], the resulting process corresponds to a marked point process (MPP) on the product space $\mathbb{R}^2 \times \mathbb{R}^+$ with intensity $\lambda f_X(x)$ [17]. A MPP $\widetilde{\Phi}$ can be formalized as a pair (φ, x) [11] and defined as

$$\widetilde{\Phi} = \{(\varphi, x); \varphi \in \Phi\}, \tag{5}$$

where φ is the point location (an element of the original PPP Φ) and x is the shadowed fading mark attached to it.

2.4 Approximating the aggregate interference

In this section, stochastic geometry is used to model the network deployments [17,19], while the cumulants concept is used to recover the distribution of the aggregate CCI at tagged receiver [10,18]. As pointed out in [11], a point process is often characterized by the conditional probabilities of events given there exist a point of the process in a specific location—the typical point. The Palm probability [20] formalizes this concept of conditioning on a point of the process, while the Campbell's theorem is used to compute the associated moment measures ([21], Chapter 16). By using the above concepts, a mathematical framework is established to characterize the aggregate interference perceived by the tagged receiver within the observation region $\mathcal{O}$. We begin by applying Campbell's theorem [17] to determine the characteristic function (CF) of the aggregate CCI distribution for the MPP $\widetilde{\Phi}$ defined in (5).

Definition 4. *Let $I = \sum_{(\varphi,x)\in\widetilde{\Phi}} p_r$ be a RV representing the interference perceived by the tagged receiver from active transmitters, and $j = \sqrt{-1}$ be the imaginary unity; then, the function $\Psi : \mathbb{R} \to \mathbb{C}$ defined as,*

$$\Psi_I(\omega) = \mathrm{E}\left[e^{j\omega I}\right], \tag{6}$$

is called the CF of I.

The corresponding n^{th} cumulant is obtained from (6) using the formulation presented in the following Proposition [10].

Proposition 1. *Let I be a RV and $\Psi_I(\omega)$ its CF. Let $n \in \mathbb{N}$. Provided that the n^{th} moment exists and is finite. Then, $\Psi_I(\omega)$ is differentiable n times and,*

$$\kappa_n\left(\widetilde{\Phi}\right) = \frac{1}{j^n}\left[\frac{\partial^n}{\partial\omega^n}\ln\Psi_I(\omega)\right]_{\omega=0}. \tag{7}$$

Proof. See ([22], Section 9.4). □

Unfortunately, there is no general closed-form expression for the PDF of the sum of LN RV, though a plethora of analytical approximations have been suggested in the literature [23-26] and references thereof. Motivated by the fact that the PDF of the aggregate interference is positively skewed [9,18], we use a single "equivalent" LN RV to approximate the summation of the individual components. The parameters of this LN approximation are estimated from the cumulants of the aggregate CCI as presented next.

$$\mu = \ln\left(\frac{\kappa_1^2}{\sqrt{\kappa_1^2+\kappa_2}}\right), \text{ and } \sigma^2 = \ln\left(1+\frac{\kappa_2}{\kappa_1^2}\right). \tag{8}$$

where μ and σ^2 are the location and scale parameters of the distribution $\mathsf{LogNormal}(\mu, \sigma^2)$, respectively.

3 Coordinated TDD-underlay

In the two-tier network under study, MBS are underlaid with standalone FBS operating in the closed access mode [2]. Communications follow two transmission schemes: (*i*) either macro and femtocells operate in the frequency division duplexing (FDD) mode where they interfere with each other on DL and UL frequency bands [27]; (*ii*) or femtocell transmissions are time multiplexed in the UL of the macrocell tier which operates in the FDD mode. In either scheme, serving cells schedule only one of their associated users per frequency-time resource block allocation (transmission interval). Furthermore, simultaneous transmissions are assumed to be synchronized and communicating nodes use omni-directional antennas. We also consider that all deployments operate under the partial co-channel configuration wherein the available spectrum is split into clear and shared parts [27] which are denoted B_c and B_s, respectively. From Figure 1, the clear part is allocated such that the macrocell traffic requirements are guaranteed, while active femtocells in the shared part compete for the remaining spectrum and are exposed to the uncoordinated CCI. Thereby, the macrocell user (MU) does not interfere with the tagged receiver but opportunistic strategies which allow femtocells to dynamically coordinate their transmissions so as to reduce the CCI are still needed. In the following, we introduce such a strategy which is based on regular busy tones [28] and

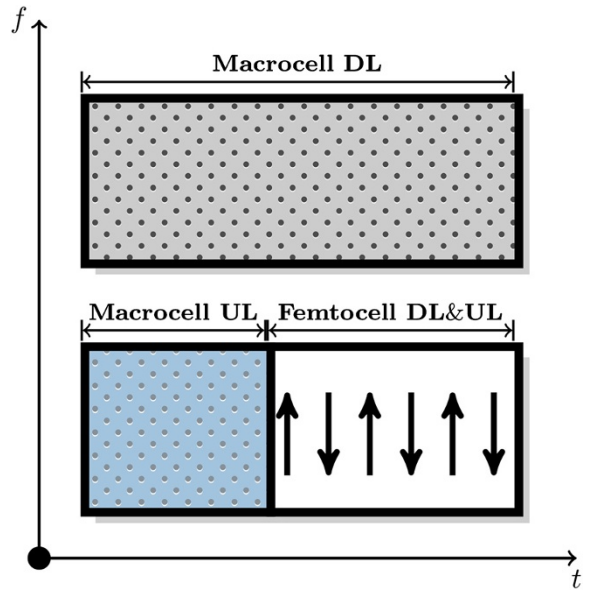

Figure 1 Spectrum arrangement. TDD-underlaid in the UL of the Macrocell tier with partial co-channel configuration [27].

enables nearby femtocells to coordinate their simultaneous transmissions. The scenarios with the coordination mechanisms are denoted as *coordinated*, whereas the *uncoordinated* term is used to designate deployments that do not use such collaborative procedures.

3.1 Coordination mechanism

Inspired by the concept of reservation busy tones which are used in [28-30] to effectively mitigate interference, we define the Coordination mechanism (CM) to control the CCI in the uncoordinated scenarios under study. Following our approach, the tagged femtocell user (FU) triggers the coordination of surrounding FBS by issuing an in-band requesting signal to advertise its presence. To achieve that, the victim user momentarily suspend its reception and transmit a requesting signal that surrounding interferers detect [5,29]. Different from the original busy burst solution whereby detecting transmitters estimate their interference parcel from the received feedback; herein, surrounding femtocells only use the busy tone as an indication of the nearby victim receiver presence. To reduce the likelihood that multiple simultaneous requests trigger the coordination procedure, an interference margin can be introduced in order to reduce the sensitivity of potential interferers to the triggering criterion. The beacon power is maintained low so as to ideally restrict the group of detecting femtocells to the dominant set of interferers. It is also worth noting that any FBS that has already triggered the coordination procedure ignores further requests that may occur while transactions related to the first request are still ongoing.

Therefore, transmitters use the CM to control their CCI parcel which is inflicted on the macrocell tier and themselves. The tagged femtocell receiver initiates the coordination procedure by experiencing the aggregate CCI above a predefined triggering threshold [31]. Notice that the network performance is assessed provided that the triggering criterion has been already satisfied. Potential interferers use the tagged receiver requesting beacon to decide about their participation in the ongoing coordination procedures. In this study, there are two distinct decision criteria which interferers employ in a distributed manner. On the one hand, potential interferers coordinate based solely on the received signal strength from the tagged receiver and we refer to it as CM1. On the other hand, we call CM2 the scenario where potential interferers use the received beacon to estimate their channel gain to the tagged receiver and then use their intending transmit power to compute the interference they would cause on that receiver similar to the busy burst solution introduced in [7]. In fact, surrounding interferers do not coordinate only by detecting the victim receiver, but use the received beacon to estimate if their interference component is above the coordination threshold ρ_{th}. Notice that the channel gain between each such interferer and the tagged receiver is assumed to be perfectly estimated (this is important to guarantee that CM2 encompasses the coordination criterion of CM1).

In the CM1, the event that surrounding interferers detect the victim receiver's beacon signal p_b above the predefined coordination threshold ρ_{th} is denoted by

$$\Upsilon_1 = \left\{ p_b R^{-\alpha} X \geq \rho_{\text{th}} \right\}. \tag{9}$$

Without loss of generality, we introduce the following indicator function,

$$\mathbb{1}_{\Upsilon_1}\left(p_b r^{-\alpha} x\right) = \begin{cases} 1 \text{ if } p_b r^{-\alpha} x \in \Upsilon_1 \\ 0 \text{ otherwise,} \end{cases} \tag{10}$$

which defines the first coordination region denoted by $\mathcal{R}_1$, and is composed of FBS that do detect under the assumptions of Υ_1 the victim receiver in their vicinity. In accordance with the formulation of Section 2.3, femtocells within this region constitute a MPP denoted by $\widetilde{\Phi}_1 = \left\{(\varphi, x) \in \widetilde{\Phi} \,|\, p_b r^{-\alpha} x \geq \rho_{\text{th}}\right\}$. Similarly, femtocells in $\mathcal{R}_2$, which do not detect the victim MU, form a process $\widetilde{\Phi}_2 = \left\{(\varphi, x) \in \widetilde{\Phi} \,|\, p_b r^{-\alpha} x < \rho_{\text{th}}\right\}$. The coordination regions $\mathcal{R}_1$ and $\mathcal{R}_2$ are disjoint and statistically independent by construction, therefore it follows immediately from the Superposition theorem [17] that $\widetilde{\Phi} = \widetilde{\Phi}_1 \cup \widetilde{\Phi}_2$. The coordination regions for Υ_2 are obtained in a similar way and the coordination criterion for the CM2 becomes,

$$\Upsilon_2 = \left\{ P R^{-\alpha} X \geq \rho_{\text{th}}, p_b R^{-\alpha} X \geq \rho_{\text{th}} \right\}. \tag{11}$$

where P yields the potential interferer's transmit power RV. With (11) we can develop an analysis similar to

the previous case and find corresponding coordination regions.

Figure 2 illustrates the non-coordination region $\mathcal{R}_2$ for both coordination criteria. It is worth noticing that after coordinating, the tagged receiver is only interfered by active transmitters in $\mathcal{R}_2$, since nodes in $\mathcal{R}_1$ switch to non-conflicting resource allocations.

4 Evaluation scenarios

Herein, we apply the framework of Section 2 to compute the aggregate interference in distinct evaluation scenarios. These scenarios are identified by the transmission mode (either FDD or TDD) and by the coordination mechanism used by nodes to autonomously avoid interference. In the UL of such scenarios, higher-order statistics are used to characterize CCI distribution at the tagged receiver. Campbell's theorem is employed to determine the CF of the aggregate interference generated by the Poisson field of transmitters. Thereafter, Proposition 1 is used to compute the cumulants of the actual distribution of the interference perceived by the tagged receiver. Then, (8) is used to estimate the parameters of the LN approximation from the respective cumulants.

4.1 Uncoordinated scenarios

Herein, co-channel transmitters use B_s without exchanging any information about their intending transmissions. In this section, we initially address the FDD configuration and thereafter the TDD-underlay mode.

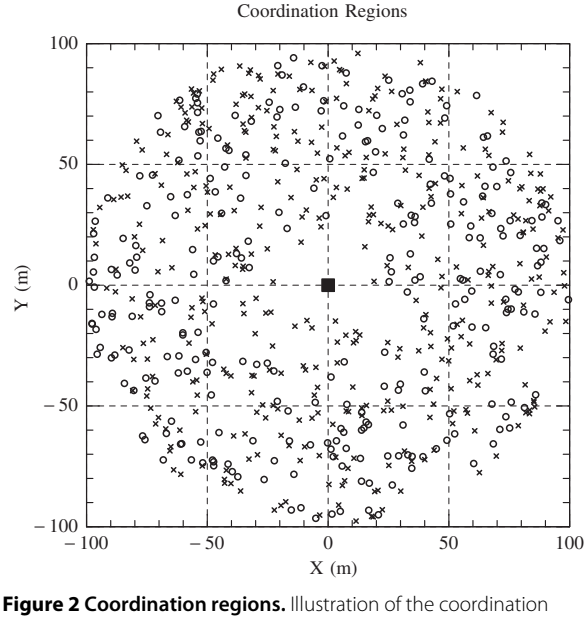

Figure 2 Coordination regions. Illustration of the coordination regions. The circles identify interferers within $\mathcal{R}_2$ after coordinating with CM1, while crosses represent non-detecting interferers by following CM2. The black shaded square identifies the tagged FBS at the origin.

4.1.1 FDD mode

In this uncoordinated deployment, FU transmit in the FDD mode lacking any sort of coordination with other co-channel transmitters in surrounding femtocells. As a consequence, communicating links are exposed to the highest interference levels. The resulting uncoordinated IP1 accounts for the interference that is caused by interferers within $\mathcal{O}$ and belonging to the point process $\widetilde{\Phi}$ as defined by (5). The n^{th} cumulant is computed as follows.

Proposition 2. *Consider the IP1; then, the n^{th} cumulant of the aggregate CCI perceived by the tagged receiver within $\mathcal{O}$ and with respect to $\widetilde{\Phi}$ is given by,*

$$\kappa_n\left(\widetilde{\Phi}\right) = \frac{2\pi\lambda p^n}{n\alpha - 2}\left({R_m}^{2-\alpha n} - {R_M}^{2-\alpha n}\right)\mathrm{E}_X\left[0,\infty,n\right]. \tag{12}$$

Proof. See Appendix 1. □

4.1.2 TDD-underlay mode

This is an uncoordinated deployment where FU are time multiplexed in the UL of the macrocell tier. Without loss of generality, we assume that the tagged receiver operates in the first of the two slots which compose the UL frame structure [6]. The aggregate interference is represented by IP2 and is caused by transmitters which operate in the first time slot within $\mathcal{O}$ and belong to the point process $\widetilde{\Phi}$ with intensity $\vartheta\lambda f_X(x)$. Hence, by observing that transmitters independently access either slot with equal probability ($\vartheta = 50\%$) and that all interfering nodes communicate with the fixed transmit power p, we extend the result in (12) to derive the cumulants for the uncoordinated TDD-underlay case as follows.

Corollary 1. *Under the assumption of the IP2, the n^{th} cumulant of the aggregate CCI perceived by the tagged receiver within $\mathcal{O}$ and with respect to $\widetilde{\Phi}$ is given by,*

$$\kappa_n\left(\widetilde{\Phi}\right) = \frac{2\pi\vartheta\lambda p^n}{n\alpha - 2}\left({R_m}^{2-\alpha n} - {R_M}^{2-\alpha n}\right)\mathrm{E}_X\left[0,\infty,n\right]. \tag{13}$$

4.2 Coordinated scenarios

In these scenarios, self-organizing femtocells coordinate with nearby potential interferers so as to reduce the overall CCI. When operating in the FDD mode, femtocells use the coordination criterion 1, while in the TDD underlay the femtocell tier benefits from both criteria as described in Section 3.

4.2.1 FDD mode with CM1

In this scenario, femtocells coordinate through the CM of Section 3 given that Υ_1 is satisfied. In the FDD mode, UL and DL operate over distinct frequency bands which gives

rise to uncorrelated fading between beacon and data (signaling and communication) channels. We consider that data and signaling channels have shadowed fading with composite Gamma and LN distributions and are indicated by independent and identically distributed RV X and Y, respectively. The remaining CCI at the tagged receiver is characterized by IP3 and its n^{th} cumulant is,

Proposition 3. *Consider the IP3, then the n^{th} cumulant of the aggregate CCI perceived by the tagged receiver in $\mathcal{O}$ with respect to $\widetilde{\Phi}_2$ has the following form,*

$$\kappa_n\left(\widetilde{\Phi}_2\right) = \frac{2\pi\vartheta\lambda\, p^n \mathrm{E}_X\left[0,\infty,n\right]}{n\alpha-2}\left\{\left(R_m^{2-\alpha n} - R_M^{2-\alpha n}\right)\right.$$
$$\times F_Y\left(R_m^{\alpha}\varrho_{\text{th}}\right) + \varrho_{\text{th}}^{n-\frac{2}{\alpha}}\mathrm{E}_Y\left[R_m^{\alpha}\varrho_{\text{th}}, R_M^{\alpha}\varrho_{\text{th}}, \frac{2}{\alpha}-n\right]$$
$$\left. - R_M^{2-n\alpha}\left[F_Y\left(R_M^{\alpha}\varrho_{\text{th}}\right) - F_Y\left(R_M^{\alpha}\varrho_{\text{th}}\right)\right]\right\}. \quad (14)$$

where $\varrho_{\text{th}} = \frac{\rho_{\text{th}}}{p_b}$ is the normalized coordination threshold.

Proof. See Appendix 2. □

4.2.2 TDD-underlay with CM1

In this scenario, femtocells still follow the coordination criterion Υ_1 as indicated in (9). Recall that the coordination is carried out through in-band signaling exchange, so that data and signaling channels are fully correlated (channel reciprocity). As described in Section 3, non-detecting femtocells of $\widetilde{\Phi}_2$ in $\mathcal{R}_2$ constitute the remaining set of interferers identified by IP4.

Proposition 4. *Consider the IP4, then the n^{th} cumulant of the aggregate CCI perceived by the tagged receiver in $\mathcal{O}$ with respect to $\widetilde{\Phi}_2$ has the following form,*

$$\kappa_n\left(\widetilde{\Phi}_2\right) = \frac{2\pi\vartheta\lambda\, p^n}{n\alpha-2}\left\{\left(R_m^{2-\alpha n} - R_M^{2-\alpha n}\right)\mathrm{E}_X[-\infty,\tilde{\varrho}_m,n]\right.$$
$$\left. + \varrho_{\text{th}}^{n-\frac{2}{\alpha}}\mathrm{E}_X\left[\tilde{\varrho}_m,\tilde{\varrho}_M,\frac{2}{\alpha}\right] - R_M^{2-n\alpha}\mathrm{E}_X\left[\tilde{\varrho}_m,\tilde{\varrho}_M,n\right]\right\}. \quad (15)$$

Proof. See Appendix 3. □

4.2.3 TDD-underlay with CM2

This scenario is represented by the IP5 wherein transmitters decide whether or not to coordinate based on their interference contribution to the aggregate CCI at the tagged receiver [7]. Working under the assumption that Υ_2 is met, the coordination procedure is carried out in the two following steps. After detecting the tagged receiver, intending transmitters rely on the channel reciprocity and use the received beacon strength to estimate their channel attenuation to that victim receiver. Thereafter, transmitters adapt their link to meet the minimum requirement of their desired receivers and still being able to transmit together with the tagged link. The standard power control (PC) algorithm is used by FU to adjust their power so as to compensate for the desired receiver channel attenuations [32]. We assume that FU are uniformly distributed within the transmission range of serving cells which schedule a random user in every transmission interval. The transmit power is set as a function of the distance between transmitter and receiver pairs, but independently of the interference at that receiver.

Lemma 1. *Under the assumptions given above, the distribution of the femtocells transmit power is,*

$$f_P(p) = \frac{1}{\alpha\beta^{1/\alpha}}p^{-1+1/\alpha}f_R\left[(p/\beta)^{1/\alpha}\right] \quad (16)$$

where $d_M = (p_M/\beta)^{1/\alpha}$ is the radio range of FBS, such that the received power at the desired user is β, p_m, and p_M are the minimum and maximum FU transmit powers, respectively, and $d_m = 1$ m is the minimum distance between an FU and its serving FBS.

Proof. Let P and R be RV representing the FBS transmit power and the distance to a random user within range, respectively. The PC fully compensates for the desired channel attenuations (channel inversion), so that $P = \beta R^{\alpha}$. The density function of R is $f_R(r) = 2r/(r_M^2 - r_m^2)$, where the radii r_m and r_M define an annular region centered at a serving femtocell. Thereby, after using the standard procedure of the change of variates in probability theory, we obtain (16). □

The n^{th} cumulant of the resulting aggregate CCI is then written as follows,

Proposition 5. *Consider the IP5, then the n^{th} cumulant of the aggregate CCI perceived by the tagged receiver in $\mathcal{O}$ with respect to $\widetilde{\Phi}_2$ has the following form,*

$$\kappa_n\left(\widetilde{\Phi}_2\right) = \frac{2\pi\vartheta\lambda}{n\alpha-2}\left[\mathcal{T}_1 + \mathcal{T}_2 - \mathcal{T}_3\right] \quad (17)$$

where $\mathcal{T}_1$, $\mathcal{T}_2$, and $\mathcal{T}_3$ are derived in Appendix 4.

Proof. See Appendix 4. □

4.3 Approximating the aggregate CCI

For each one the evaluation scenarios, the analytical framework of Section 2.4 is used to recover the respective aggregate CCI. In this example, the observation region is determined with $R_m = 1$ m and $R_M = 100$ m. The density of interferers is $\lambda = 0.05$ FBS/m^2. As aforesaid, when operating in the TDD-underlay mode, femtocells choose either slot with equal probability $\vartheta = 50\%$. The radio

channel is affected by path loss with exponent $\alpha = 3$, LN shadowing with $\sigma_{\text{dB}} = 6\,\text{dB}$, and Nakagami fading with shape factor $m = 16$. In the femtocell tier, transmitters use a fixed power level of $p = 20\,\text{dBm}$. When using PC with full compensation, femtocells control their transmit power to fully compensate for the average value of the desired receivers' large-scale fading.

Figure 3 compares the CCDF of the aggregate CCI from Monte Carlo simulations with those from the LN. As can be seen from these figures, the LN approximation matches quite well with the simulation results, though the proposed approximations work slightly better with lower fading variance ($m = 16$). In the coordinated scenarios, a coordination threshold of $\rho_{\text{th}} = -40\,\text{dBm}$ and an MU requesting power of $p_b = 0\,\text{dBm}$ are used. Comparing the aggregate CCI of uncoordinated scenarios with that of coordinated ones, we observe that the two-tier networks under study benefit most from avoiding dominant interferers through the CM. Indeed, the coordinated cases provide gains due to the formation of dynamic exclusion regions around the tagged receiver.

5 Performance analysis

We evaluate the performance of the scenarios under study in terms of the outage probability and average channel capacity with respect to the tagged receiver. Next, closed-form expressions to approximate the aforementioned figures of merit are introduced.

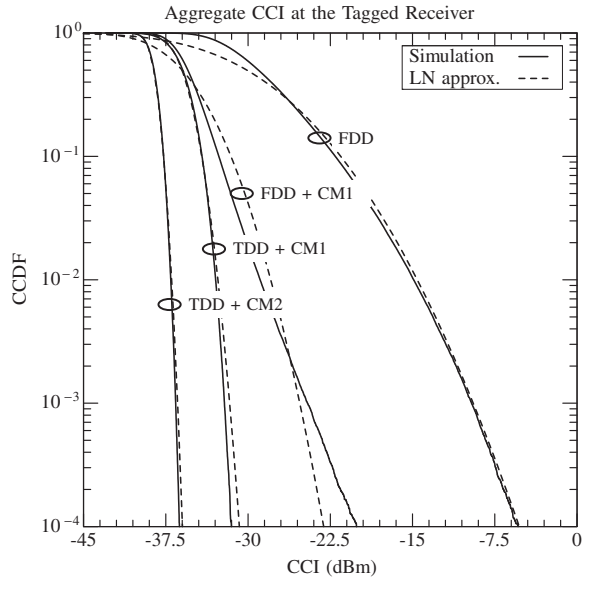

Figure 3 Aggregate CCI at the tagged receiver. Complementary cumulative distribution function (CCDF) of the aggregate CCI at the tagged FBS under shadowed fading with $\sigma_{\text{dB}} = 6\,\text{dB}$ and $m = 16$ (corresponds to a Rician factor $K = 14.8\,\text{dB}$).

5.1 Signal-to-interference ratio and outage probability

The outage probability is given by $\Pr[\Gamma < \gamma_{\text{th}}]$, where Γ is the perceived signal-to-interference ratio (SIR) at the tagged receiver, and γ_{th} is the SIR detection threshold. Notice that the scenarios under study are interference limited and hence the thermal noise is negligible in comparison to the resulting CCI [33].

Theorem 1. *Let Z_0 and Z be LN RV representing the power received from the tagged transmitter and the aggregate CCI at the tagged receiver, respectively. Under the assumption of the shadowed fading with composite Gamma-LN distribution, the SIR at the tagged receiver is*

$$\Gamma \sim \text{LogNormal}\left(\mu_{V_0} - \mu_V, \sigma_{V_0}^2 + \sigma_V^2\right), \tag{18}$$

and the outage probability is given by

$$\Pr\{\Gamma < \gamma_{\text{th}}\} = \text{Q}\left[\left(\mu_{SIR} - \gamma_{\text{th}}\right)/\sigma_{SIR}\right]. \tag{19}$$

Proof. The SIR distribution is given by the quotient of two independent LN RV, namely, $Z_0 = e^{V_0}$ that is the power received from the tagged transmitter, and $Z = e^{V}$ that is an equivalent LN RV approximating the aggregate CCI at the tagged receiver. Hence, we apply the multiplicative reproductive property of LN RV to obtain the SIR distribution [34]. □

5.2 Average spectral efficiency

We also evaluate how the CM perform in the two-tier coexistence scenarios by means of the location-dependent average channel capacity of the tagged receiver [35]. By using the analytical framework previously established, and assuming that all users are allocated on the same bandwidth, W, we initially recover the SIR distribution of the tagged receiver, and then compute the corresponding capacity.

Theorem 2. *Under the assumption of the shadowed fading channel regime, the average channel capacity of the tagged receiver is given as,*

$$\bar{C} \simeq W \sum_{k=1}^{K} \frac{\omega_k}{\sqrt{\pi}} \log_2\left[1 + \exp\left(\frac{\eta_k\sqrt{2}\sigma + \mu}{\xi}\right)\right]. \tag{20}$$

Proof. To compute the location-dependent average channel capacity,

$$\bar{C} = W \int_0^{\infty} \log_2(1+\gamma) f_{\Gamma}(\gamma)\, \text{d}\gamma, \tag{21}$$

we use the PDF of the SIR with respect to the tagged receiver, which is indicated by $f_{\Gamma}(\gamma)$.

To do that, we use the Gauss-Hermite quadrature [10],

$$\int_{-\infty}^{+\infty} e^{-\eta^2} f(\eta)\, d\eta = \sum_{k=1}^{K} \omega_k f(\eta_k) + R_K, \tag{22}$$

where η_k is the k^{th} zero of the Hermite polynomial $H_K(\eta)$ of degree K, ω_k is the corresponding weight of the function $f(\cdot)$ at the k^{th} abscissa, and R_K is the remainder value. K corresponds to the number of sample points which are used to approximate $f(\eta)$ [10,26]. After that, by using the substitution $\eta = (\xi \ln \gamma - \mu)/\sqrt{2}\sigma$ in (21), we obtain expression (20). □

5.3 Numerical results

Herein, we consider the same assumptions and configuration parameters of Section 4.3. In Figure 4, we use Theorem 1 to plot the outage probability for an increasing density of FU. The uncoordinated scenarios present the poorest performance, while in the time-multiplexing scenario the tagged receiver experiences slightly better performance since the CCI is reduced by a factor that is proportional to the number of time-slots available in a UL frame. By avoiding the dominant interferers through the coordination procedure, the tagged receiver performance significantly improves, whereas the extent of the coordination gains depend on the correlation between beacon and data channels. When nodes coordinate by fulfilling Υ_1, the time-multiplexed scenarios outperform the typical FDD transmission mode. However, by comparing the coordination criteria in the TDD-underlay case, we observe an interesting trade-off between individual link quality and overall spectrum efficiency. In fact, when nodes coordinate following the criterion given by Υ_1, the tagged receiver experiences better link quality since less interferers are active. However, when nodes follow Υ_2, the overall utilization of radio resources is increased since more simultaneous transmissions are allowed at the expense of slightly worse outage figures for the tagged link.

We use Theorem 2 to present the ergodic capacity of the tagged link for an increasing density of interfering nodes in Figure 5. As previously observed with the outage probability, the coordinated scenarios outperform the uncoordinated ones. The uncoordinated TDD-underlay case presents ergodic channel capacity comparable to the FDD deployment with the CM1. Moreover, by assessing the configuration with TDD-underlay and CM2, it becomes clear that the tagged link experiences lower average channel capacity owing to the higher number of simultaneous transmission which are allowed in this case.

6 Conclusions and final remarks

In this article, we address the CCI problem in two-tier coexistence scenarios. As opposed to the typical spectrum partitioning approaches, the TDD concept is assessed as an alternative to underlay short-range femtocell communications on the UL of legacy macrocell deployments. Herein, we consider distributed mechanisms based on the regular busy tones and that rely on minimal signaling exchange to coordinate the underlaid femtocell tier to reduce the co-channel interference. An analytical framework based on stochastic geometry and higher-order statistics through the cumulants concept which captures network dynamics and channel variations is introduced. We use this framework to recover the distribution of the

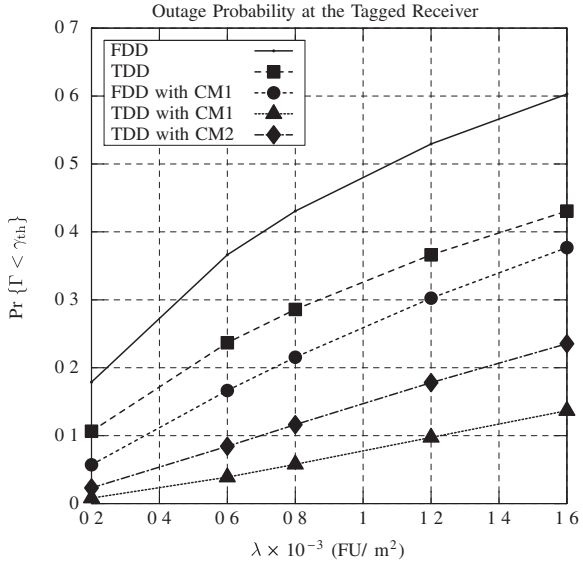

Figure 4 Outage probability. Outage probability at the tagged receiver for increasing density of interfering FU. We consider a Nakagami-*m* shape parameter $m = 16$ (that corresponds to the Rice parameters $K = 14.8$ dBm) and network radius of 100 m.

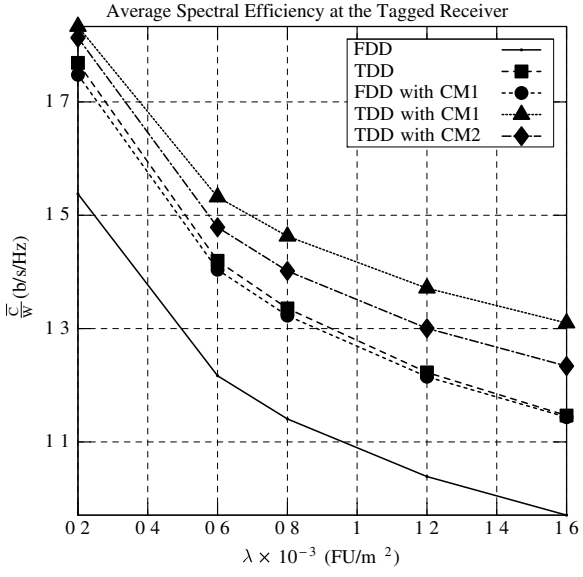

Figure 5 Average spectral efficiency. Average spectral efficiency at the tagged receiver for increasing density of interfering FU. We consider a Nakagami shape parameter $m = 16$ (that corresponds to the Rice parameters $K = 14.8$ dBm) and network radius of 100 m.

co-channel interference and to evaluate the system performance in terms of the outage probability and average spectral efficiency of the tagged link. Our analytical model matches well with numerical results obtained using Monte Carlo simulations. When compared to the uncoordinated FDD deployment, the outage probability of the evaluation scenarios with the coordinated TDD-underlay solution is reduced by nearly 80%, while the average spectral efficiency increases by approximately 90% at high loads.

Appendix 1

Proof of Proposition 2

Using Definition 4, the CF of the aggregate CCI perceived by the tagged receiver is written as

$$\Psi_I(\omega) = \exp\left\{2\pi \int_0^{\infty}\int_{R_m}^{R_M} \left[\exp\left(jwpr^{-\alpha}x\right) - 1\right] \times \lambda f_X(x)\, r\, \mathrm{d}r\, \mathrm{d}x\right\}. \quad (23)$$

By evaluating (7) using (23), and integrating with respect to r, we obtain

$$\kappa_n\left(\widetilde{\Phi}\right) = \frac{2\pi\lambda p^n}{n\alpha - 2}\left({R_m}^{2-\alpha n} - {R_M}^{2-\alpha n}\right)\int_0^{\infty} x^n f_X(x)\mathrm{d}x, \quad (24)$$

as the n^{th} cumulant of the CCI distribution. Since transmissions are affected by the shadowed fading, the LN approximation of Section 2.4 is used with Definition 3 to obtain $\mathrm{E}_X[0,\infty,n] = e^{n\mu+\frac{1}{2}n^2\sigma^2}$ and from there derive (12).

Appendix 2

Proof of Proposition 3

Considering interfering FBS in $\mathcal{R}_2$, the n^{th} cumulant of the aggregate interference is determined from the CF as follows

$$\Psi_I(\omega) = \exp\left\{2\pi \int_0^{\infty}\int_0^{\infty}\int_{R_m}^{R_M} \left[\exp\left(jwp_t r^{-\alpha}x\right) - 1\right] \times \lambda f_X(x) f_Y(y)\, \mathbb{1}_{\Upsilon_1^c}\left(r^{-\alpha}y\right) r\mathrm{d}r\, \mathrm{d}y\, \mathrm{d}x\right\}, \quad (25)$$

where $\Upsilon_1^c = 1 - \Upsilon_1$ corresponds to the event of not detecting a victim receiver.

The n^{th} cumulant is then given by

$$\begin{aligned}\kappa_n &= 2\pi\lambda \int_0^{\infty}\int_0^{\infty}\int_{\max\left[R_m,(y/\varrho_{\text{th}})^{1/\alpha}\right]}^{R_M} p^n r^{1-n\alpha} x^n f_X(x) \times f_Y(y)\mathrm{d}r\,\mathrm{d}y\,\mathrm{d}x \\ &= 2\pi\lambda p^n \int_X x^n f_X(x)\,\mathrm{d}x\left[\int_0^{\varrho_m}\int_{R_m}^{R_M} r^{1-n\alpha} f_Y\left(y\right)\mathrm{d}r\,\mathrm{d}y \right. \\ &\quad \left. + \int_{\varrho_m}^{\varrho_M}\int_{(y/\varrho_{\text{th}})^{1/\alpha}}^{R_M} r^{1-n\alpha} f_Y\left(y\right)\mathrm{d}r\,\mathrm{d}y\right]. \end{aligned} \quad (26)$$

where $\varrho_{\text{th}} = \rho_{\text{th}}/p_b$, $\varrho_m = \varrho_{\text{th}} R_m^{\alpha}$ and $\varrho_M = \varrho_{\text{th}} R_M^{\alpha}$. By integrating (26) with respect to r, we obtain

$$\begin{aligned}\kappa_n &= \frac{2\pi\lambda\, p^n \mathrm{E}_X[0,\infty,n]}{n\alpha - 2}\left\{\left(R_m^{2-\alpha n} - R_M^{2-\alpha n}\right)\int_{-\infty}^{\varrho_m} f_Y(y)\mathrm{d}y \right. \\ &\quad \left. + \int_{\varrho_m}^{\varrho_M}\left[y^{\frac{2}{\alpha}-n}\varrho_{\text{th}}^{n-\frac{2}{\alpha}} - R_M^{2-n\alpha}\right] f_Y(y)\mathrm{d}y\right\}. \end{aligned} \quad (27)$$

Finally, we obtain the expression (14) after computing the partial moments of the approximating LN RV X and Y by repeatedly applying Definition 3, and by using the change of variable $Y = e^{\mu+\sigma Z}$, where $Z \sim \text{Normal}(0,1)$, along with the substitutions $\tilde{\varrho}_M = \frac{\ln \varrho_M - \mu}{\sigma}$ and $\tilde{\varrho}_m = \frac{\ln \varrho_m - \mu}{\sigma}$.

Appendix 3

Proof of Proposition 4

By considering the indicator function in (10), we write the CF of the aggregate CCI for the $\mathcal{R}_2$ as,

$$\Psi_I(\omega) = \exp\left\{2\pi \int_0^{\infty}\int_{R_m}^{R_M} \left[\exp\left(jwpr^{-\alpha}x\right) - 1\right] \times \vartheta\lambda f_X(x)\, \mathbb{1}_{\Upsilon_1^c}\left(r^{-\alpha}x\right) r\mathrm{d}r\mathrm{d}x\right\}. \quad (28)$$

And from (7), the n^{th} cumulant is

$$\begin{aligned}\kappa_n &= 2\pi\vartheta\lambda \int_0^{\infty}\int_{\max\left[R_m,(x/\varrho_{\text{th}})^{1/\alpha}\right]}^{R_M} (p)^n r^{1-n\alpha} x^n f_X(x)\mathrm{d}r\,\mathrm{d}x \\ &= 2\pi\vartheta\lambda\left[\int_{\varrho_M}^{\infty}\int_{R_m}^{R_M} (p)^n r^{1-n\alpha} x^n f_X(x)\mathrm{d}r\,\mathrm{d}x \right. \\ &\quad \left. + \int_{\varrho_m}^{\varrho_M}\int_{R_m}^{(x/\varrho_{\text{th}})^{1/\alpha}} (p)^n r^{1-n\alpha} x^n f_X(x)\mathrm{d}r\,\mathrm{d}x\right]. \end{aligned} \quad (29)$$

Similar to the derivation of (27), we first integrate with respect to r and obtain

$$\begin{aligned}\kappa_n &= \frac{2\pi\vartheta\lambda\, p^n}{n\alpha - 2}\left\{\left(R_m^{2-\alpha n} - R_M^{2-\alpha n}\right)\int_{\varrho_M}^{\infty} x^n f_X(x)\mathrm{d}x \right. \\ &\quad \left. + \int_{\varrho_m}^{\varrho_M}\left[x^n R_m^{2-n\alpha} - x^{\frac{2}{\alpha}}\varrho_{\text{th}}^{n-\frac{2}{\alpha}}\right] f_X(x)\mathrm{d}x\right\} \end{aligned} \quad (30)$$

Likewise the previous case, after computing the following partial moments with respect to X, and using the change of variable $X = e^{\mu+\sigma Z}$, we obtain the expression (15).

$$\mathrm{E}_X[-\infty, \varrho_m, n] = e^{n\mu+\frac{n^2\sigma^2}{2}}\left(1 - \mathrm{Q}[\tilde{\varrho}_m - n\sigma]\right), \tag{31}$$

$$\mathrm{E}_X\left[\varrho_m, \varrho_M, \frac{2}{\alpha}\right] = e^{\frac{2\mu}{\alpha}+\frac{2\sigma^2}{\alpha^2}}\left(\mathrm{Q}\left[\tilde{\varrho}_m - \frac{2\sigma}{\alpha}\right] - \mathrm{Q}\left[\tilde{\varrho}_M - \frac{2\sigma}{\alpha}\right]\right), \tag{32}$$

$$\mathrm{E}_X[\varrho_m, \varrho_M, n] = e^{n\mu+\frac{n^2\sigma^2}{2}}\left(\mathrm{Q}\left[\tilde{\varrho}_m - n\sigma\right] - \mathrm{Q}\left[\tilde{\varrho}_M - n\sigma\right]\right), \tag{33}$$

where $\mathrm{Q}[u] = \frac{1}{\sqrt{2\pi}}\int_u^\infty e^{-\frac{v^2}{2}}\,\mathrm{d}v$.

Appendix 4

Proof of Proposition 5

By using the indicator function of (11), we write the CF of the aggregate CCI for the resulting $\mathcal{R}_2$ as,

$$\Psi_I(\omega) = \exp\left\{2\pi\int_{p_m}^{p_M}\int_0^\infty\int_{R_m}^{R_M}\left[\exp\left(jwpr^{-\alpha}x\right) - 1\right] \times \vartheta\lambda f_X(x) f_P(p)\,\mathbb{1}_{\Upsilon_2}\left(pr^{-\alpha}x\right) r\mathrm{d}r\mathrm{d}x\mathrm{d}p\right\}. \tag{34}$$

And from (7), the corresponding n^{th} cumulant becomes

$$\begin{aligned}\kappa_n &= 2\pi\vartheta\lambda\int_0^\infty\int_{\max\left[R_m,(xp/\rho_{\text{th}})^{1/\alpha}\right]}^{R_M} p^n r^{1-n\alpha}x^n f_X(x) f_P(p) \times \mathrm{d}r\,\mathrm{d}x\,\mathrm{d}p \\ &= 2\pi\vartheta\lambda\left[\int_{p_m}^{p_M}\int_{\frac{\varrho_M}{p}}^\infty\int_{R_m}^{R_M} p^n r^{1-n\alpha}x^n f_X(x)\mathrm{d}r\,\mathrm{d}x\,\mathrm{d}p \right. \\ &\quad \left. + \int_{p_m}^{p_M}\int_{\varrho_m}^{\varrho_M}\int_{(xp/\rho_{\text{th}})^{1/\alpha}}^{R_M} p^n r^{1-n\alpha}x^n f_X(x) f_P(p)\mathrm{d}r\,\mathrm{d}x\,\mathrm{d}p\right],\end{aligned} \tag{35}$$

where $\rho_m = \rho_{\text{th}}R_m^\alpha$ and $\rho_M = \rho_{\text{th}}R_M^\alpha$. After integrating (35) with respect to r, we obtain

$$\begin{aligned}\kappa_n = \frac{2\pi\vartheta\lambda}{n\alpha-2}&\left[\left(R_m^{2-\alpha n} - R_M^{2-\alpha n}\right)\int_{p_m}^{p_M}\int_{\rho_M/p}^\infty p^n x^n f_X(x) \times f_P(p)\mathrm{d}x\,\mathrm{d}p + \int_{p_m}^{p_M}\int_{\rho_m/p}^{\rho_M/p}\left(p^n x^n R_m^{2-n\alpha}\right.\right. \\ &\left.\left. - p^{\frac{2}{\alpha}}x^{\frac{2}{\alpha}}\rho_{\text{th}}^{n-\frac{2}{\alpha}}\right) f_X(x) f_P(p)\mathrm{d}x\,\mathrm{d}p\right]\end{aligned} \tag{36}$$

Using the change of variate from Appendix 2 we can rewrite the cumulant expression as,

$$\kappa_n = \frac{2\pi\vartheta\lambda}{n\alpha-2}\left[\mathcal{T}_1 + \mathcal{T}_2 - \mathcal{T}_3\right] \tag{37}$$

where $\tilde{\rho}_M = \frac{\ln(\rho_M/p)-\mu}{\sigma}$, $\tilde{\rho}_m = \frac{\ln(\rho_m/p)-\mu}{\sigma}$, and

$$\begin{aligned}\mathcal{T}_1 &= \left(R_m^{2-\alpha n} - R_M^{2-\alpha n}\right)\int_{p_m}^{p_M} p^n e^{n\mu+\frac{n^2\sigma^2}{2}}\left(1-\mathrm{Q}[\tilde{\rho}_m - n\sigma]\right) \times f_P(p)\mathrm{d}p, \\ \mathcal{T}_2 &= \int_{p_m}^{p_M} p^n R_m^{2-n\alpha} e^{\frac{2\mu}{\alpha}+\frac{2\sigma^2}{\alpha^2}}\left(\mathrm{Q}\left[\tilde{\varrho}_m - \frac{2\sigma}{\alpha}\right] - \mathrm{Q}\left[\tilde{\varrho}_M - \frac{2\sigma}{\alpha}\right]\right) f_P(p)\,\mathrm{d}p, \\ \mathcal{T}_1 &= \int_{p_m}^{p_M} p^{\frac{2}{\alpha}}\rho_{\text{th}}^{n-\frac{2}{\alpha}} e^{n\mu+\frac{n^2\sigma^2}{2}}\left(\mathrm{Q}\left[\tilde{\varrho}_m - n\sigma\right] - \mathrm{Q}\left[\tilde{\varrho}_M - n\sigma\right]\right) \times f_P(p)\,\mathrm{d}p.\end{aligned} \tag{38}$$

The cumulant in (37) can be computed in a closed form expression, but unfortunately it is final format is overly cumbersome. Thereby, we decide to simply indicate the corresponding operation in (17).

Competing interests

The authors declare that they have no competing interests.

Acknowledgements

Authors would like to thank the Finnish funding agency for technology and innovation (Tekes), Elektrobit, Renesas Mobile, and Nokia Siemens Networks for supporting this study. This study had been also conducted in the framework of the ICT project ICT-4-248523 BeFEMTO, which is partly funded by the EU.

Received: 21 November 2011 Accepted: 23 November 2012
Published: 2 January 2013

References

1. H Claussen, L Ho, L Samuel, An overview of the femtocell concept. Bell Labs Tech. J. **13**, 221–245 (2008)
2. V Chandrasekhar, JG Andrews, A Gatherer, Femtocell networks: a survey. Commun. Mag., IEEE. **46**(9), 59–67 (2008)
3. CHM de Lima, M Bennis, M Latva-aho, in *Globecom Global Telecommunications Conference (GLOBECOM 2011), 2011 IEEE*. Coordination mechanisms for stand-alone femtocells in self-organizing deployments, (Houston, TX, USA, 2011), pp. 1–6
4. D López-Pérez, A Valcarce, G de la Roche, J Zhang, OFDMA femtocells: a roadmap on interference avoidance. Commun. Mag., IEEE. **47**(9), 41–48 (2009)
5. S Rangan, in *Globecom*. Femto-macro cellular interference control with subband scheduling and interference cancelation, (Miami, Florida, USA, 2010), pp. 695–700
6. Z Bharucha, H Haas, in *67th IEEE Vehicular Technology Conference (VTC), 2008. VTC Spring 2008. IEEE*. Application of the TDD underlay concept to home NodeB scenario, (Calgary, Canada, 2008), pp. 56–60
7. P Omiyi, H Haas, G Auer, Analysis of TDD cellular interference mitigation using busy-bursts. Wireless Commun., IEEE Trans. on. **6**(7), 2721–2731 (2007)
8. H Inaltekin, M Chiang, HV Poor, SB Wicker, On unbounded path-loss models: effects of singularity on wireless network performance. Sel. Areas Commun., IEEE J. on. **27**(7), 1078–1092 (2009)
9. MJ Ho, GL Stüber, Capacity and power control for CDMA microcells. ACM J. Wirel. Netw. **1**(3), 355–363 (1995)
10. M Abramowitz, IA Stegun, *Handbook of Mathematical Functions with Formulas, Graphs, and Mathematical Tables*, edn., vol. 69 (Dover, 1965)
11. A Baddeley, I Bárány, R Schneider, W Weil, *Stochastic Geometry* (Springer, 2006)
12. J Illian, A Penttinen, H Stoyan, D Stoyan, *Statistical Analysis and Modelling of Spatial Point Patterns* (Wiley-Interscience, 2004)

13. F Baccelli, B Btaszczyszyn, in *Stochastic Geometry and Wireless Networks—Theory,* vol. 1 of *Foundations and Trends in Networking*, ed. by F Baccelli, B Blaszczyszyn. NoW—The essence of knowledge (NoW Publishers, 2009), p. 209
14. F Baccelli, B Btaszczyszyn, in *Stochastic Geometry and Wireless Networks—Applications,* vol. 2 of *Foundations and Trends in Networking*, ed. by F Baccelli, B Blaszczyszyn. NoW—The essence of knowledge (NoW Publishers, 2009), p. 150
15. J Andrews, R Ganti, M Haenggi, N Jindal, S Weber, A primer on spatial modeling and analysis in wireless networks. Commun. Mag., IEEE. **48**(11), 156–163 (2010)
16. P Xia, V Chandrasekhar, JG Andrews, Open vs. closed access femtocells in the uplink. Wireless Commun., IEEE Trans. on. **9**, 3798–3809 (2010)
17. JFC Kingman, *Poisson Processes* (Oxford University Press, 1993)
18. A Ghasemi, ES Sousa, Interference aggregation in spectrum-sensing cognitive wireless networks. Sel. Topics Signal Process., IEEE J. of. **2**, 41–56 (2008)
19. D Stoyan, WS Kendall, J Mecke, *Stochastic Geometry and Its Applications*, 2nd edn. (Wiley-Blackwell, 1995)
20. F Baccelli, P Bremaud, *Elements of Queueing Theory*, 2nd edn. (Springer, 2003)
21. AE Gelfand, P Diggle, P Guttorp, M Fuentes (eds.), *Handbook of Spatial Statistics* (CRC Press, 2010)
22. S Resnick, *A Probability Path* (Birkhäuser, Boston, 1999)
23. NC Beaulieu, Q Xie, An optimal lognormal approximation to lognormal sum distributions. Vehicular Technol., IEEE Trans. on. **53**(2), 479–489 (2004)
24. L Felton, An optimal lognormal approximation to lognormal sum distributions. IRE Trans. Commun. Systs. **8**, 57–67 (1960)
25. JCSS Filho, P Cardieri, MD Yacoub, Simple accurate lognormal approximation to lognormal sums. Electron. Lett. **41**(18), 5–6 (2005)
26. J Wu, NB Mehta, J Zhang, in *Globecom*. A flexible lognormal sum approximation method, (St. Louis, MO, 2005), pp. 3413–3417
27. 3GPP: Home Node B Radio Frequency RF Requirements (FDD). Tech. rep., TR25.967, version 9.0.0 release 9 (2009)
28. H Haas, V Nguyen, P Omiyi, N Nedev, G Auer, in *2006 IEEE International Conference on Communications*. Interference aware medium access in cellular OFDMA/TDD networks, (2006), pp. 1778–1783
29. S Sinanovic, G Auer, H Haas, in *IEEE Globecom*. Power control and interference awareness using busy bursts, (Anchorage, Alaska, USA, 2010), pp. 1–5
30. S Sinanovic, G Auer, H Haas, in *IEEE Globecom*. Interference analysis of busy burst enabled interference avoidance, (Miami, Florida, USA, 2010), pp. 1–5
31. S Sinanovic, H Burchardt, N Serafimovski, G Auer, H Haas, in *IEEE International Conference on Communications*. Local information busy burst thresholding, (2009), pp. 1–6
32. 3GPP: Radio Resource Control (RRC); Protocol specification. Tech. rep., TS25.331, version 10.5.0 release 10 (2011)
33. S Weber, J Andrews, N Jindal, An overview of the transmission capacity of wireless networks. Commun., IEEE Trans. on. **58**(12), 3593–3604 (2010)
34. M Dale, *The Algebra of Random Variable* (Wiley & Sons, Inc., 1979)
35. WCY Lee, Estimate of channel capacity in rayleigh fading environment. **39**(3), 187–189 (1990)

doi:10.1186/1687-1499-2013-3
Cite this article as: de Lima *et al.*: **Coordinated TDD-Underlay for Self-organizing Femtocells in Two-Tier Coexistence Scenarios.** *EURASIP Journal on Wireless Communications and Networking* 2013 **2013**:3.